

1
2
3
4
5
6
7
8
9
10
11
12
13
14
15
16
17
18
19
20
21
22
23
24
25
26
27
28
29

Small-Molecule Modulators of Lipid Raft Stability and Protein-Raft Partitioning

Authors

Katherine M. Stefanski^{1,2}, Hui Huang^{1,2}, Dustin D. Luu³, James M. Hutchison⁴, Nilabh Saksena^{1,2}, Alexander J. Fisch^{1,2}, Thomas P. Hasaka^{1,5}, Joshua A. Bauer^{1,5}, Anne K. Kenworthy⁶, Wade D. Van Horn³, Charles R. Sanders^{1,2*}

Affiliations

- ¹Department of Biochemistry, Vanderbilt University School of Medicine, Nashville, Tennessee, USA.
- ² Center for Structural Biology, Vanderbilt University School of Medicine, Nashville, Tennessee, USA.
- ³ School of Molecular Sciences; The Virginia G. Piper Biodesign Center for Personalized Diagnostics, Arizona State University, Tempe, AZ, USA.
- ⁴ Department of Pharmacology, Yale University School of Medicine, New Haven, CT 06520, USA; Yale Cancer Biology Institute, Yale University West Campus, West Haven, CT, USA.
- ⁵ Vanderbilt Institute of Chemical Biology, High-Throughput Screening Facility, Vanderbilt University School of Medicine, Nashville, Tennessee, USA.
- ⁶ Center for Membrane and Cell Physiology and Department of Molecular Physiology and Biological Physics, University of Virginia School of Medicine, Charlottesville, VA, USA.

*Corresponding author. Email chuck.sanders@vanderbilt.edu (C.S.)

30 **Abstract**

31 Development of an understanding of membrane nanodomains colloquially known
32 as “lipid rafts” has been hindered by a lack of pharmacological tools to manipulate rafts
33 and protein affinity for rafts. We screened 24,000 small molecules for modulators of the
34 affinity of peripheral myelin protein 22 (PMP22) for rafts in giant plasma membrane
35 vesicles (GPMVs). Hits were counter-screened against another raft protein, MAL, and
36 tested for impact on raft , leading to two classes of compounds. Class I molecules
37 altered the raft affinity of PMP22 and MAL and also reduced raft formation in a protein-
38 dependent manner. Class II molecules modulated raft formation in a protein-
39 independent manner. This suggests independent forces work collectively to stabilize
40 lipid rafts. Both classes of compounds altered membrane fluidity in cells and modulated
41 TRPM8 channel function. These compounds provide new tools for probing lipid raft
42 function in cells and for furthering our understanding of raft biophysics.

43
44 **Teaser**

45 Compounds have been discovered that modulate the affinity of membrane
46 proteins for lipid rafts as well as raft formation.

47
48
49
50

51 **MAIN TEXT**

52

53 **Introduction**

54

55 Lipid rafts are dynamic phase-separated nanodomains of the plasma membrane
56 that are thicker and more rigid than the bulk membrane and are typically enriched in
57 cholesterol and in phospholipids with saturated acyl chains, often sphingolipids (1–4). It
58 has long been theorized that cells utilize lipid rafts as sorting and signaling platforms (5–
59 10). Specific proteins are thought to partition into rafts under cellular conditions where
60 they facilitate a variety of biological functions. Lipid rafts have been implicated in
61 immune signaling, neural development, host-pathogen interactions, caveolae,
62 cytoskeletal-membrane contacts, and other cellular phenomena (11–15). Under
63 physiological conditions lipid rafts in cells are believed to be nanoscale and highly
64 dynamic, severely limiting traditional microscopic studies (16–18).

65 Giant plasma membrane vesicles (GPMVs) derived from the plasma membranes
66 of live cells are a well-established tool for studying lipid rafts and for quantitating the raft
67 affinity of membrane proteins (19). GPMVs are easy to prepare and will spontaneously
68 phase separate into micron-scale liquid ordered (L_o , raft) and liquid disordered (L_d , non-
69 raft) domains. Assorted fluorescent dyes or protein markers are available to label
70 ordered and disordered phases in GPMVs, enabling imaging-based analysis of phases
71 and resident proteins. GPMVs also retain the lipid and protein composition of the cell
72 plasma membrane from which they are derived (20, 21).

73 The affinity of a number of membrane proteins for lipid rafts relative to the
74 surrounding disordered phase has been assessed in GPMVs. GPMVs have also been
75 used to elucidate the characteristics that drive raft affinity (22–24). A majority of the

76 membrane proteins thought to preferentially partition into lipid rafts are single-span
77 proteins. Studies of single-span raft-avid proteins enabled the identification of structural
78 criteria for raft affinity. Palmitoylation, transmembrane domain length, and surface area
79 are the main drivers of raft partitioning for single-pass membrane proteins (22). No such
80 rules have been determined for multispan proteins, in large part because only a small
81 number of raft-favoring multispan proteins have been unambiguously identified, and the
82 rules for single-pass proteins do not seem to apply (23, 25).

83 Peripheral myelin protein 22 (PMP22) is a tetraspan membrane protein that
84 preferentially partitions into ordered domains in GPMVs. PMP22 is highly expressed in
85 myelinating Schwann cells and is a major component of myelin in the peripheral
86 nervous system (PNS). Duplication of the PMP22 gene causes the most common type
87 1A form of Charcot-Marie-Tooth (CMT) disease (26), a peripheral neuropathy that is a
88 top 10 most common genetic disorder. More severe forms of CMT are caused by
89 inherited point mutations in PMP22 (27). While the biophysical properties that drive
90 PMP22 into lipid rafts are unknown, an analysis of disease-associated PMP22
91 mutations in GPMVs revealed that most of the mutations resulted in reduced protein
92 preference for the raft phase versus the disordered phase (25). The fact that the tested
93 disease mutants are known to destabilize protein folding suggests raft affinity is
94 dependent on the fold of PMP22 (28). Given that PMP22 is thought to be involved in
95 supporting cholesterol homeostasis and trafficking in Schwann cells, it is very possible
96 that its affinity for lipid rafts is closely related to one of its key physiological functions in
97 forming healthy myelin (29). These considerations motivated us to seek compounds that

98 alter PMP22 raft affinity, thereby providing tools for use in investigating the drivers and
99 physiological consequences of PMP22 raft partitioning.

100 We conducted high throughput screening (HTS) to discover molecules that
101 alter PMP22 phase partitioning between ordered and disordered domains. Our primary
102 assay reports not only on PMP22 phase partitioning, but also on whether compounds
103 alter raft formation. Here we report the discovery of small molecules falling into two
104 classes. Class I compounds decreased the affinity for lipid rafts of PMP22 and myelin
105 and lymphocyte protein (MAL) [another raft-preferring tetraspan membrane protein
106 (23)]. Class I compounds also reduced raft formation in a protein-dependent manner.
107 Class II compounds altered raft formation independent of proteins. Both classes of
108 compounds were seen to alter membrane fluidity in GPMVs and live cells. We further
109 explored their activities by examining their effects on the activity of the human cold-
110 sensing TRPM8 channel and on signaling by the epidermal growth factor receptor
111 (EGFR). These compounds provide new tools for investigating raft-dependent
112 phenomena in cells. Additionally, the differing modes of action of these compounds
113 expand our understanding of raft biophysics.

114 115 **Results**

116 117 **A high-throughput screen identifies compounds that alter PMP22 raft affinity**

118 To identify compounds that alter the ordered domain partitioning of PMP22 we
119 conducted a high-throughput screen adapted from our recent method (Fig. 1) (25).
120 Briefly, the goal was to use GPMVs from cells expressing PMP22 to screen for small
121 molecules that alter the proportion of PMP22 in the ordered phase. GPMVs were made
122 from transfected HeLa cells expressing PMP22. We employed the N41Q (glycosylation

123 deficient) variant of PMP22 since it traffics to the plasma membrane with much higher
124 efficiency than wild type (WT) but exhibits the same ordered domain preference (25,
125 31). The disordered phase was labeled with the lipophilic stain Dil while PMP22 was
126 immunolabeled with AlexaFluor 647. GPMVs were deposited into 96 or 384-well plates
127 containing compounds at a final concentration of 10 μ M. A 23,360 compound sub-set of
128 the >100,000 compound Vanderbilt Discovery Collection and a library of FDA approved
129 drugs (1,184) were screened. The Discovery collection compounds represents a cross-
130 section in terms of the chemical diversity of the master library. Plates were imaged
131 using a high-content spinning disc confocal imaging system. VesA software was used to
132 analyze images (30). The power of this approach is in the number of vesicles that can
133 be imaged and analyzed in an unbiased manner. A typical well results in images
134 containing thousands of GPMVs which are then analyzed automatically, independent of
135 investigator bias or foreknowledge. Hits from the screen were picked using strictly
136 standardized mean difference (SSMD) values on a plate-by-plate basis (typical cutoff
137 was an SSMD value $\geq 90\%$ of the positive control) based on compound impact on
138 PMP22 $P_{ordered}$ (32). $P_{ordered}$ is the fraction of protein in the ordered phase and is a
139 measure of the affinity of a particular protein for rafts. An initial hit rate of 1.06% was
140 observed, resulting in 267 preliminary hits. Hits were then confirmed in triplicate
141 experiments using compounds from the library. Compounds of interest were then
142 reordered from the manufacturer and their effects confirmed. Validated compounds
143 were then tested in GPMVs from cells expressing the MAL protein, another lipid raft-
144 preferring tetraspan protein (23), to test whether their activity is protein-specific.

145 Effects of all hits on raft formation were also measured. Here we used the
146 fraction of phase-separated GPMVs (vs non phase-separated) in our images as a
147 measure of raft formation. For all confirmed compound hits (above), we also completed
148 measurements in GPMVs from untransfected cells. Hits fell into several distinct
149 categories based on these data criteria. In this work, we focus on two interesting
150 functional classes of compounds.

151

152 **Protein-dependent modulators of raft affinity and raft stability (Class I molecules)**

153 Among the validated hits, two compounds were found to have unique effects on
154 both protein raft affinity and raft formation. VU0615562 and VU0619195 significantly
155 decreased $P_{ordered}$ for both PMP22 and MAL by ~18-20% (Figs. 2A and 2B). While
156 PMP22 and MAL are tetraspan myelin proteins with a known affinity for lipid rafts they
157 have little-or-no sequence homology. These compounds thus reduce $P_{ordered}$ for two
158 non-homologous tetraspan membrane proteins.

159 Dose-response experiments indicated that EC_{50} values for the impact of the two
160 compounds on each protein are in the ~1 μ M range (Figs. 2C and 2D). To verify the
161 effects of the compounds are not specific to HeLa cells we confirmed similar activities in
162 GPMVs derived from rat basophilic leukemia (RBL) cells which also produce GPMVs
163 that phase separate at temperatures that are feasible for our microscopes (fig. S1).

164 We next examined the effects of VU0615562 and VU0619195 on raft stability in
165 GPMVs derived from untransfected cells and from cells expressing either PMP22 or
166 MAL. We used the fraction of phase-separated vesicles from images (c.f., Fig. 2E) as a
167 proxy for raft formation. The compounds decreased the fraction of phase-separated

168 GPMVs in all cases (Figs. 3A and 3B, gray bars). However, when PMP22 or MAL were
169 overexpressed, this reduction in phase-separated vesicles was significantly more
170 pronounced compared with GPMVs from untransfected cells (Figs. 3A and 3B) and was
171 observed across a range of concentrations (Fig. 3C, curve does not approach 0 as in
172 Figs. 3D and 3E). For both compounds the EC₅₀ values were in the vicinity of 1 μM.
173 This led us to speculate that these compounds reduce raft stability via a mechanism
174 that is not specific to a single protein but is dependent on the presence of proteins. We
175 hypothesize that the activity of the compounds observed in GPMVs from untransfected
176 cells is because the compounds exploit endogenous membrane proteins in HeLa cells
177 to exert their effects.

178 We know that PMP22 expression stabilizes ordered domains (25) so the
179 augmented effect size of raft destabilization observed in GPMVs + PMP22 seems to be
180 the consequence of an intrinsic property of VU0615562 and VU0619195 that is
181 somehow enhanced when PMP22 is present. To determine if MAL has a similar effect
182 on raft formation in the absence of Class I compounds we used data from within the
183 same images and compared the fraction of phase-separated vesicles from MAL positive
184 (GFP+) and MAL negative (GFP-) GPMVs (a feature of the VesA software allows us to
185 make this distinction). We used DMSO treated control wells from dose-response
186 experiments for this comparison. In contrast to PMP22 (25), in compound-free samples
187 we found that MAL expression has very little impact on phase separation (fig. S2).
188 These data indicate that the enhancement of Class I compound raft destabilization by
189 PMP22 or MAL reflects an intrinsic activity of these compounds that is enhanced by the
190 presence of the proteins via an unknown mechanism.

191 To further investigate this apparent protein dependence, we tested the impact of
192 these compounds on GPMVs treated with proteinase K. Proteinase K is a broad-
193 spectrum serine protease capable of cleaving proteins preferentially after hydrophobic
194 residues. Note that it has been previously shown that GPMVs can be porous, so it is
195 likely both intracellular and extracellular loops and segments are cleaved by the
196 protease (33). We applied this treatment to GPMVs from untransfected cells because
197 the protease activity would eliminate our ability to label or detect PMP22 or MAL (by
198 cleaving the myc tag or GFP fusion), obviating our ability to differentiate GPMVs
199 containing either protein. We found that proteinase K treatment significantly reduced the
200 effects of the compounds (Fig. 3F). This supports the conjecture that the changes
201 induced by the compounds are not specific to any one protein but are dependent on the
202 presence of multiple proteins (overexpressed and/or endogenous). The incomplete
203 effect of proteinase K in reducing the raft-lowering activities of these compounds may
204 be due to its inability to digest all membrane proteins present completely. However,
205 these data, combined with the results seen with PMP22 and MAL led us to conclude
206 that multiple proteins have the trait of being able to enhance the ordered phase
207 destabilizing effects of VU0615562 and VU0619195.

208 To be certain that the compounds were not remodeling the GPMVs we examined
209 the size of GPMVs and the size of the ordered phases when treated with the
210 compounds. Neither GPMV radii nor relative sizes of ordered phase domains were
211 changed by VU0615562 or VU0619195 (figs. S3A and S3B), even though they
212 decrease the raft affinities of PMP22 and MAL, as well as raft formation.

213 An examination of the chemical structures of VU0615562 and VU0619195 (Table
214 1) reveals a Tanimoto coefficient (a metric of chemical similarity ranging from 0-1) of
215 0.7778 (34). This chemical similarity is unsurprising in light of their similar effects on
216 $P_{ordered}$ for PMP22 and MAL, as well as raft formation. Since these compounds were
217 similar, structure-activity relationship (SAR) studies were conducted on chemically
218 similar compounds available in the VU Discovery Collection (fig. S4). For VU0615562,
219 seven additional compounds with similar structures (similarity integer value of 97) were
220 tested. For VU0619195, six additional compounds with similar structures (similarity
221 integer value of 85) were tested. None of the compounds tested had a greater impact
222 on PMP22 ordered partitioning or raft stability than VU0615562 and VU0619195 (fig.
223 S4). It is interesting, however, that for both compounds, analogs were found that
224 maintained the capacity of the parent compound to reduce the raft affinity of PMP22
225 while largely losing their ability to reduce raft formation, suggesting that these two
226 activities are incompletely coupled.

227

228 **Protein-independent raft modulators (Class II)**

229 It is reasonable to wonder if the protein-dependent raft modulating effects
230 described above for VU0615562 and VU0619195 are unique to these compounds or if
231 all raft modulating compounds would show a similar dependence in their activities on
232 proteins. This turned out not to be the case based for three other compounds
233 discovered in the initial screen for compounds that altered $P_{ordered}$ for PMP22. These
234 compounds have variable effects on the ordered partitioning of PMP22. VU0615562
235 and VU0619195 have little-or-no effect on the partitioning of MAL (fig. S5A), but lower

236 P_{ordered} for PMP22 in RBL cells (fig. S1A) and possibly in HeLa cells (albeit without
237 statistical rigor, see Fig. 4A). The third compound, primaquine diphosphate, increases
238 P_{ordered} for both MAL (Fig. 4A and fig. S5B) and PMP22 in HeLa cells (Fig. 4A), but not
239 in RBL cells (fig. S1A).

240 Two of these compounds—VU519975 and VU607402— decreased raft formation
241 in GPMVs (Fig. 4B, fig. S5C) while the FDA-approved drug, primaquine diphosphate
242 (PD), increases raft formation (Fig. 4B, figs. S1B and S5D). These compounds are
243 chemically dissimilar (Table 2). Importantly, unlike the case for Class I compounds, the
244 presence of PMP22 (Fig. 4B) or MAL (fig. S5C) did not dramatically alter the effects of
245 these compounds on raft formation. The independence of the activity of the compounds
246 on proteins is supported by experiments with GPMVs from untransfected cells treated
247 with proteinase K. The activities of these compounds were not sensitive to proteolysis
248 (Fig. 4C). Taken together, we conclude that these compounds are raft modulators that
249 likely interact with the membrane in a protein-independent manner. EC_{50} values for
250 impact on raft stability in GPMVs could not be reliably determined for VU519975 and
251 VU607402 since they were seen to be insoluble in GPMV buffer at concentrations
252 above 15 μM (Fig. 4D), whereas the EC_{50} for the effect of PD on raft stability in GPMVs
253 was determined to be roughly 2.1 μM (Fig. 4E).

254 Neither VU519975, VU607402, nor PD affect GPMV size or the relative size of
255 ordered domains in GPMVs (fig. S6A-D). PD does induce a small but significant
256 decrease in the size of PMP22-containing ordered domains (figs. S6D-bottom panel and
257 S6E).

258 When interpreting any effect on raft formation it is important to factor in the
259 impact of temperature. For example, we found that the impact of PD treatment on raft
260 stability at 27 °C compared to 23 °C was significantly larger (a 125% increase vs a 12%
261 increase) (fig. S5D). See Methods for additional details about this effect and
262 considerations for data interpretation.

263

264 **Class I and II compounds alter membrane fluidity in GPMVs and live cells**

265 We examined the effects of all five compounds (both classes, biophysical effects
266 summarized in Table 3) on membrane fluidity to potentially shed light on how they
267 impact on raft stability. Because fluidity experiments can be conducted in live cells this
268 approach also provided an opportunity to connect GPMV findings with raft behavior of
269 plasma membranes in living cells. For this, we used the environmentally sensitive dye
270 Di-4-ANEPPDHQ (Di-4) to report on membrane fluidity (35). Increased membrane
271 fluidity causes a red-shift of the Di-4 emission spectrum; whereas, blue-shifted spectra
272 arise from decreased fluidity.

273 First, we treated GPMVs derived from HeLa cells incubated with each compound
274 and Di-4 and then measured emission spectra. For the four raft destabilizing
275 compounds, a pronounced red-shift from vehicle was observed in micrographs (Fig. 5A)
276 and in measured emission spectra (Fig. 5B). To quantify these changes, generalized
277 polarization (GP) values were determined (Fig. 5C). GP values provide a relative means
278 of comparing spectral shifts. For Di-4 emission, lower values correspond to a more fluid
279 (red-shifted) environment. Decreased GP values for the four raft destabilizing

280 compounds indicate a significant increase in membrane fluidity. While there was a small
281 increase in GP from PD treatment the change in fluidity was not statistically significant.

282 All data presented thus far were collected in GPMVs and, therefore do not inform
283 whether the compounds exert effects in living cells. To address this, we repeated the
284 fluidity measurements with Di-4 in live cells. HeLa cells were treated with compounds
285 ~15 min before a brief incubation with Di-4 to limit internalization of the dye and ensure
286 primarily plasma membrane labeling. Cells were then imaged via laser scanning
287 confocal microscopy using a spectral detector, allowing images from multiple emission
288 wavelengths to be simultaneously acquired (Fig. 5D and fig. S7A. GP values were then
289 calculated from the confocal microscopy data. We found that the changes in GP were
290 very similar to those from GPMVs, with more variability in living cells (Fig. 5E). Two
291 compounds, VU0619195 (Class I) and VU0607402 (Class II), produced statistically
292 significant increases in membrane fluidity. We also added methyl- β -cyclodextrin
293 (MBCD) to HeLa cells to deplete membranes of cholesterol and increase membrane
294 fluidity. In comparison to addition of VU0619195 and VU0607402, the effect of MBCD
295 treatment was modest. While not statistically significant, the effects of VU0615562,
296 VU0519975, and PD on Di-4 emission in live cells show similar changes relative to each
297 other as in the GPMV Di-4 experiments (Fig. 5, compare C and E).

298 Qualitatively, the MBCD-treated cells also appeared rounded (fig. S7, bottom
299 row) compared to the hit compound-treated cells, which retained the well spread
300 appearance of untreated cells, suggesting that the compounds reported here are better
301 tolerated by live cells than MBCD treatment. Trypan blue cell viability experiments
302 confirmed that MBCD shows toxicity in cells while none of the 5 compounds of this work

303 were cytotoxic (fig. S7B) at the concentrations and timescales used in the live cell
304 experiments of this study. These compounds provide improved tools for manipulating
305 lipid rafts in living cells in studies of the functional relevance of lipid rafts in different
306 biological processes, both by being more effective at increasing membrane fluidity and
307 also by being less toxic. Knowing that the effects of the compounds discovered in this
308 work extend to the plasma membranes of living cells, we were motivated to investigate
309 their impact on putative raft-dependent functions of selected membrane proteins.

310

311 **Compounds alter TRPM8 channel activity but not autophosphorylation of EGFR**

312 To test if Class I and Class II compounds could alter a reported lipid raft-
313 dependent biological outcome, we examined their effects on the human TRPM8 ion
314 channel function. TRPM8 is a cold and menthol sensing ion channel (36, 37). Many ion
315 channels, including TRPM8, are thought to associate with lipid rafts and have signaling
316 properties that are thought to be sensitive to being in or out of rafts (38–40). We
317 conducted automated patch clamp (APC) electrophysiology experiments (Fig. 6A, fig.
318 S8A) to determine if compound treatment altered TRPM8 function. TRPM8-expressing
319 cells were equilibrated to 30 °C (41) and treated with the canonical TRPM8 agonist
320 menthol before and after 15 minutes of continuous perfusion with the lipid raft
321 modulating compounds. Comparisons of the pre- and post-menthol-stimulated currents
322 were used to evaluate the effects of the raft-modulating compounds on TRPM8 function.
323 As with the fluidity experiments, MBCD was included for comparison since previously
324 published studies used MBCD to deplete cholesterol and disrupt lipid rafts. We found
325 that perfusion with VU0619195 (Class I), VU0607402 (Class II), and MBCD reduced the

326 TRPM8 current responses to menthol stimulation (Fig. 6B, fig. S8B). This result
327 supports the notion that TRPM8 function is dependent on lipid rafts and/or changes in
328 membrane fluidity. PD, (class II, increases raft stability) did not significantly alter TRPM8
329 activity. These results are similar to those seen in the live-cell fluidity experiments and
330 provides important cross-validation.

331 The addition of VU0619195, VU0607402, and PD did not alter cell surface levels
332 of TRPM8 as quantified by flow cytometry (fig. S8C). Interestingly, MBCD increased the
333 level of surface TRPM8, which may be a consequence of its known activity as an
334 inhibitor of endocytosis (42).

335 We also examined the impact of compounds on the activation of the epidermal
336 growth factor receptor (EGFR) by epidermal growth factor (EGF). Previous studies have
337 shown changes in EGFR activation following disruption of lipid rafts by MBCD treatment
338 (43–45). We treated HeLa cells with VU0619195, VU0607402, or PD for 15 minutes (as
339 in the TRPM8 experiments) prior to a brief (1 min) treatment with EGF. Cells were then
340 lysed and levels of EGFR phospho-tyrosine 1173 and phospho-ERK (which is
341 phosphorylated downstream of EGFR phosphorylation) were quantified via Western blot
342 analysis. We did not see significant effects on either EGFR or ERK phosphorylation
343 (Fig. 6C, fig. S9), indicating that these signaling processes are not sensitive to short-
344 term changes in membrane fluidity or raft modulation. These data also indicate that not
345 all plasma membrane signaling events are sensitive to the changes in lipid raft stability
346 induced by these compounds. These EGFR data provide a useful counterexample to
347 the findings that TRPM8 function is altered by these raft-modulating compounds.

348
349

350 **Discussion**

351
352 HTS led to the discovery of five novel lipid raft modulating small molecule
353 compounds falling into two classes that modulate different features of lipid raft stability.
354 Two compounds function as protein-dependent raft destabilizers that also reduced the
355 lipid raft affinity of both PMP22 and MAL (Class I). This a novel class of small molecules
356 whose modality, to our knowledge, has never previously been reported. We also
357 identified two protein-independent raft destabilizers and one protein-independent raft
358 stabilizer that also enhance the lipid raft affinity of both PMP22 and MAL (Class II). That
359 lipid rafts can be manipulated via protein-dependent and protein-independent
360 interactions is notable. This suggests that there are independent lipid and protein-based
361 stabilizing forces that work together to promote ordered domain formation. The
362 compounds exerted effects both in isolated plasma membrane vesicles and in live-cell
363 plasma membranes. They also altered the signaling of a raft-sensitive ion channel,
364 TRPM8.

365 Commonly used methods for altering lipid rafts in cells include removal or
366 delivery of cholesterol via MBCD and use of alcohols of varying chain lengths (46–48).
367 These approaches each have limitations. MBCD efficiently removes cholesterol, but this
368 is ultimately lethal to cells. MBCD is also not specific and can remove phospholipids as
369 well as cholesterol (47). Hexadecanol and octanol can be used to decrease or increase
370 membrane fluidity, respectively (46), but they have low miscibility in aqueous buffers
371 and media, making them challenging to work with in cell-based assays. We also
372 recently described bioactive compounds that promote and reduce raft formation, but the
373 previously-reported compounds are all known to have effects on various cellular

374 functions for which they were originally described (for example, one is a protease
375 inhibitor) (30). Here we have presented new small molecules, two of which induce a
376 more robust increase in membrane fluidity than MBCD, all of which were observed to be
377 non-toxic under experimental conditions. These compounds should therefore be useful
378 tools for manipulating lipid raft formation and raft-partitioning of membrane proteins in
379 biophysical and cell biological studies.

380 Potential applications for these compounds are exemplified in our studies with
381 TRPM8 and EGFR. Prior studies implicated lipid raft localization as having regulatory
382 effects on the activities of both TRPM8 and EGFR (43, 44, 49). Our results showed that
383 compounds that decrease raft formation robustly decrease TRPM8 signaling. We note
384 that previous studies reported an *increase* in rat TRPM8 channel activity after treatment
385 with MBCD (41, 50). The difference in phenotype is likely the result of speciation
386 difference between the human TRPM8 used in this study compared to the rat TRPM8
387 used in the previous studies (51, 52). Speciation differences have also been seen in
388 various other TRP channels, including TRPA1, TRPV3, and TRPV1 (53, 54)

389 Reduced raft formation induced by treatment with the same compounds that
390 affected TRPM8 had little to no effect on EGFR phosphorylation, in contrast to the
391 reported impact of lipid raft disruption by MCBBD treatment (43, 44, 55). This suggests
392 that EGFR activity may be more sensitive to the cholesterol concentration in the
393 membrane than it is to lipid rafts. Examples of membrane proteins that sense and are
394 regulated by lipids are replete in the literature. Some G protein-coupled receptors are
395 known to be allosterically regulated by direct binding of cholesterol (56). Another
396 example is provided by prior work on the yeast transcriptional regulator Mga2, which

397 demonstrated that some proteins sense acyl chain composition rather than overall
398 fluidity and respond with a rotational conformational change that regulates their activity
399 (57).

400 Further studies will need to be conducted to establish the exact mechanisms by
401 which the five compounds reported in this work exert their effects. The data suggest that
402 the two Class I protein-dependent compounds work to change protein raft affinity and
403 phase separation by altering protein-lipid interactions in a manner that may be partly but
404 incompletely coupled to changes in membrane fluidity. They may intercalate into the
405 membrane at protein lipid-interfaces and disrupt raft promoting interactions. The
406 discovery of these compounds supports previous assertions that proteins play a critical
407 role in regulating lipid rafts (58, 59). The three Class II protein-independent compounds
408 likely work by inserting into the membrane and altering lipid packing and changing
409 membrane fluidity (60, 61). We have no reason to suspect that these compounds
410 change the lipid composition (as MBCD does) on the short time scales (15 minutes)
411 they were tested, and given their structures. However, future lipidomic analyses will test
412 this possibility. We speculate that a long-term incubation of live cells with the
413 compounds could result in some level of membrane remodeling as cells respond to the
414 changes in raft stability and membrane fluidity. Cells have adapted mechanisms to
415 sense and respond to these changes that result from natural temperature changes
416 which are believed to keep their membranes near the miscibility critical point (62–65).
417 Further experiments with the compounds can broaden our understanding of these
418 mechanisms.

419 Finally, we note that two of the Class II compounds altered the phase partitioning
420 of PMP22 in GPMVs derived from at least some cell types, while P_{ordered} for MAL
421 remained unperturbed (see Table 3 for summary). While this is a very preliminary result
422 and will require further exploration and testing, it does suggest that it should be possible
423 to discover modulators of raft affinity that are protein-specific. This would be a very
424 welcome development both for studies of how the function of specific proteins are
425 altered by raft association and potentially even for therapeutic applications.

426 Overall, the discovery of first in class molecules in this work present new tools for
427 interrogating lipid rafts and raft proteins in cells. Moreover, our initial results using these
428 compounds shed light on the fact that both protein-lipid and lipid-lipid interactions
429 combine to stabilize lipid rafts and that these can be independently manipulated.

430 **Materials and Methods**

431 **Cell culture**

432
433 HeLa and RBL-2H3 cells and were acquired from the American Tissue Culture
434 Collection (ATCC, Manassas Va, cat #CCL-2 and CRL-2256). T-REx-293 cells were
435 acquired from Invitrogen (Cat # R71007). Cells were grown at 37 °C in 5% CO₂ in a
436 humidified incubator. HeLa cells were cultured in low glucose DMEM (Gibco #
437 11885084) supplemented with 10% fetal bovine serum (FBS, Gibco, #26140-079) and
438 1% penicillin/streptomycin (P/S, Gibco, #15140-122). RBL-2H# cells were cultured in
439 MEM (Gibco 11095808) with 10% FBS and 1% penicillin/streptomycin. T-Rex-293 cells
440 were cultured in high glucose DMEM (Gibco cat # 11965092) supplemented with 10%
441 tetracycline free fetal bovine serum (Corning cat # 35-075-CV) with 1%
442 penicillin/streptomycin.
443
444

445

446 **GPMV formation and imaging**

447 HeLa cells were plated at $\sim 1.4 \times 10^6$ cells total in a 150 mm plate. For PMP22
448 experiments: 24 hrs later cells were transfected with 15 ug of pSF PMP22 N41Q-myc
449 using Fugene 6 (Promega cat # E2691) following the manufacturers protocol. Cells
450 were grown for an additional 48 hrs post transfection. In counterscreening experiments,
451 cells were transfected with a MAL-GFP construct (gift from the Levental lab (23)).
452 GPMVs were generated using a standard protocol (19), cells were first rinsed twice with
453 10 ml of inactive GPMV buffer (150 mM NaCl, 10 mM HEPES, 2 mM CaCl₂, pH7.4). To
454 label the disordered phase, cells were stained with DiI12(3) (1,1'-Didodecyl-3,3',3'-
455 Tetramethylindocarbocyanine Perchlorate) (Dil, Invitrogen cat # D383) for 10 minutes.
456 Cells were then rinsed twice again with inactive GPMV buffer then subsequently
457 incubated in 8.5-10 ml of active GPMV buffer (GPMV buffer + 2 mM DTT, 25 mM
458 formaldehyde) at 37°C for 1.5 hrs. After incubating, GPMVs in solution were collected
459 from the dish and allowed to settle at room temperature for 1 hr. 8-9 mL of GPMVs were
460 then collected by pipetting from neither the top nor the bottom of the tube to leave
461 behind both floating and settled debris. A mouse anti-myc antibody (Cell Signaling,
462 9B11) was then added at a ratio of 1:1500 and incubated for 1 hr. This was followed by
463 incubation with an anti-mouse antibody conjugated to AlexaFluor647 (Cell Signaling, cat
464 # 4410) at 1:15000. GPMVs were added to multi-well plates with compounds from
465 DMSO stocks and allowed to incubate for 1.5 hrs. Plates were then imaged on an
466 ImageXpress Micro Confocal High Content Screening System (Molecular Devices, San

467 Jose CA) with a Nikon 40X 0.95 NA Plan Apo Lambda objective and an Andor Zyla
468 4.2MP 83% QE sCMOS camera, and an 89-North LDI 5 channel laser light source.

469

470 **High-throughput screen and GPMV image analysis**

471 A pilot screen was conducted with an FDA approved drug library (1,184 compounds) by
472 testing the library plated in triplicate. Primaquine diphosphate (PD) was found to have
473 significant effects on promoting PMP22 ordered partitioning and increasing raft stability.
474 It was carried through the larger screen as a positive control. Compounds were
475 obtained from the Vanderbilt Discovery collection at the VU HTS core. This library
476 contains over 100,000 compounds with the first 20,000 representing the greatest
477 structural diversity. Compounds were dispensed via a Labcyte Echo 555 into 384-well
478 plates such that final the final screening concentration for all compounds was 10 μ M.
479 GPMVs were made and labeled as described above and added to the plates containing
480 compounds. The first and last columns of the plates were filled with positive and
481 negative controls. Plates were incubated for at least 1.5 hours at room temperature prior
482 to imaging. 16 images per well were collected using an IXMC as described above.
483 Images were then analyzed using VesA. Strictly standardized mean differences
484 (SSMDs) were used to calculate effect sizes for the PMP22 ordered phase partition
485 coefficient ($P_{ordered}$), for every well (32, 66). The SSMDs for positive (PD) and negative
486 (DMSO) controls were used as a benchmark to select hits from each plate. A typical
487 cutoff for selecting hits was a SSMD value of >90% of the positive control SSMD for
488 PMP22 ordered partitioning. These criteria resulted in a 1-3% hit rate. SSMD values for
489 PMP22 ordered partitioning were used to pick hits. For each hit we also noted the

490 fraction of phase-separated vesicles (also calculated by VesA). A minimum of 100
491 GPMVs expressing PMP22 per well was required to be included as a hit. Hits were then
492 screened by qualitatively assessing the images from screening. Hits that showed
493 significant visible compound precipitation or extreme changes in GPMV size/shape
494 were discarded. After screening 23,360 compounds 267 hits were identified following
495 the above criteria, reflecting a 1.06% hit rate. These hits were then tested in triplicate
496 against library compound. From hits that were validated at this phase, those with the
497 largest effects were selected and reordered from a commercial vendor (20 compounds,
498 vendor list below).

499 Experiments using reordered compounds were conducted in 96-well plate with
500 duplicate or triplicate wells (technical replicates) in each plate (biological replicate). For
501 experiments with PMP22 or MAL, GPMVs containing the overexpressed construct were
502 analyzed. For follow-up and dose response experiments, a minimum of 10 phase-
503 separated GPMVs per biological replicate were required for ordered partitioning
504 measurements (determination of $P_{ordered}$). For experiments without PMP22 or MAL,
505 (untransfected cells) all GPMVs were analyzed.

506

507 **Compound repurchasing**

508 Compounds from the Vanderbilt Discovery Collection were reordered from Life
509 Chemicals (VU0615562, Cat. No. F3382-6184) (VU0619195, Cat. No. F3398-2024)
510 (VU0519975, Cat No. F5773-0110) (VU0607402, Cat. No. F3255-0148) (Niagara on the
511 Lake, Ontario, Canada). PD was acquired from Selleckchem (Cat. No. S4237)
512 (Houston, TX, USA).

513

514 **Dose-response experiments**

515 GPMVs from cell expressing or not expressing PMP22 or MAL were prepared and
516 labeled as described above. Doses of hit compounds or DMSO were made by serial
517 dilution and deposited into wells of a 96-well plate for a final concentration from 0.01 to
518 15 μM . The measured fraction of phase-separated GPMVs and $P_{ordered}$ were normalized
519 to DMSO controls and averaged. Curves were fit in GraphPad Prism10 and half
520 maximal effective concentrations (EC_{50}) were determined using a non-linear sigmoidal
521 model.

522

523 **Proteinase K treatment**

524 Protease treatment of GPMVs was conducted as previously described (67). GPMVs
525 were made from untransfected HeLa as described above and labeled with DiD and
526 NBD-PE. GPMVs were then separated into 2 tubes. One tube was treated with 20
527 $\mu\text{g}/\text{mL}$ of proteinase K (Macherey-Nagel cat #740506). Proteinase K and untreated
528 GPMVs were incubated for 45 min at 37°C . 2 mM PMSF was added to quench the
529 proteinase K treatment. GPMVs were then added to wells in a 96-well plate containing
530 compounds for a final concentration of 10 μM . GPMVs were imaged and analyzed as
531 described above.

532

533 **Temperature considerations when working with GPMVs**

534 With the following exception, all of the work presented thus far was carried about at 21-
535 23 $^\circ\text{C}$. Phase separation is highly temperature dependent and previous work found that

536 the temperature at which half of GPMVs from HeLa cells phase separate is roughly 25
537 °C (25). The instrument used for most of this work is limited at low end of temperature to
538 about 21°C. So, we could not easily probe the effect size of raft destabilizing
539 compounds by further decreasing the temperature (which would increase phase
540 separation). Our ability to heat samples was less restricted. In addition to the altered
541 effects on raft stability in response to PD treatment, there was also a more modest
542 increase in MAL ordered partitioning at 27 °C vs 23 °C (fig. S5C). This illustrates that
543 temperature is a crucial variable to consider when interpreting the effects of these
544 compounds on raft stability and ordered partitioning.

545

546 **Plate reader membrane fluidity assay**

547 For fluidity measurements in GPMVs, GPMVs were made as described above without
548 any staining prior to vesiculation. Once collected and settled, GPMVs were stained with
549 Di-4-ANEPPDHQ (Invitrogen, cat # D36802). To optimize the concentration of each
550 stain a pilot study was conducted with 0.1% DMSO and single compound and dye
551 concentrations ranging from 0.5 µM to 10 µM. From this, 1 µM as determined to give the
552 best effect sizes for Di-4. For experiments with all compounds GPMVs were treated with
553 dye then deposited in wells of a 96-well plate with compounds (10 µM final for each
554 compound) and incubated at room temperature for about 40 minutes. After incubation
555 the plate was read on a SpectraMax iD3 plate reader (Molecular Devices). Data were
556 acquired using SoftMax Pro 7 version 7.1.0 (Molecular Devices). Di-4 was excited at
557 470 nm and emission spectra were collected from 550 to 800 nm using 2 nm steps. The
558 photomultiplier tube gain was set to automatic with an integration time of 140 ms.

559
$$(1) GP = \frac{I_B - I_R}{I_B + I_R}$$

560 From the spectra, generalized polarization values were calculated with Equation 1.

561 Where I_B is a value in the blue end of the emission spectra and I_R is a value at the red
562 end. For Di-4 565 nm and 605 nm were selected for I_B and I_R respectively.

563

564 **Image-based membrane fluidity assays**

565 For imaging, GPMVs were prepared, treated with compounds, and labeled with Di-4 in
566 the same manner as described in the previous section. They were seeded in an 8-well
567 chamber slide with a coverslip on the bottom (Ibidi cat # 80806). Images were acquired
568 on a Zeiss LSM 880 laser scanning confocal using a spectral detector and a 40X oil
569 immersion objective. Images were collected at emission wavelengths from 410 nm to
570 689.5 nm at an interval of 8.9 nm.

571 Live-cell experiments were conducted by first seeding 10,000 cells per well in 8-
572 well chamber slides. The following day, 1 hr prior to imaging, cells treated to deplete
573 cholesterol were first rinsed with serum-free media then incubated with 10 mM methyl-
574 β -cyclodextrin (MBCD) in serum-free DMEM. After 30 minutes at 37 C, cells were
575 removed from the incubation and treated with 10 μ M compounds in serum-free CO₂
576 independent media (Gibco L15 media, # 2108302) for 30 min. (MBCD treated well was
577 also swapped from 10 mM MBCD in serum-free CO₂ independent media). Prior to
578 imaging, Di-4 was added to a final concentration of 2 μ M. Imaging and Di-4 addition
579 were staggered to ensure less than 30 min passed after addition of the dye and
580 imaging. This is in line with previous observations that Di-4 begins to accumulate in
581 endosomes after 30 min. Additionally, images were acquired at room temperature to

582 slow internalization of the dye. Imaging was conducted on the LSM 880 as described in
583 the previous section. Fluorescence intensities of individual cells were measured in
584 ImageJ across all 32 wavelengths. 2 to 3 cells were measured using Fiji (68) from 5
585 fields of view per condition. GP values were calculated as they were in the plate reader
586 assay with intensities 561.5 nm and 605.8 nm used at the blue and red values
587 respectively.

588

589 **Trypan blue cell viability**

590 To ensure that effects seen in Di-4 live cell fluidity experiments and APC experiments
591 were not due to inherent toxicity of the compounds trypan blue experiments were
592 conducted. HeLa cells were collected and treated with 10 μ M compound or 10 mM
593 MBCD as in the Di-4 assay. Live-dead staining was then conducted with trypan blue as
594 previously described (69). Cells were mixed in a 50:50 ratio with trypan blue reagent
595 then immediately quantified on an automated Countess 3 cell counter (Fisher Scientific).
596 Experiments were conducted on three separate days with measurements taken in
597 duplicate.

598

599 **Automated patch clamp electrophysiology**

600 HEK293 cells stably expressing full-length human TRPM8 were grown in DMEM media
601 (Gibco 11960077) with 10% fetal bovine serum (Gibco 16000), 4 mM L-glutamine
602 (Gibco 25030), 100 U/mL penicillin-streptomycin (Gibco 15140), 100 μ M non-essential
603 amino acid solution (Gibco 11140050), 4 mM glutaMax (Gibco 35050061), 200 μ g/mL
604 G418 (Sigma-Aldrich A1720), and 0.12% sodium bicarbonate (Gibco 25080094) at 37

605 °C and 8% CO₂ in 100 mm dishes, as previously (70). After growing to 75% confluency
606 (3-4 days), the cells were washed twice with 2 mL per dish of phosphate buffer saline
607 solution (PBS), pH 7.4 (Gibco 10010031) followed by incubation of accutase (2 mL per
608 dish, Gibco A1110501) for 5 minutes at 37 °C. Cells were then triturated and transferred
609 to a conical tube and centrifuged at 200 ×g for 1.5 min to remove the accutase. The
610 cells were resuspended with serum-free media (Gibco 11686029) and transferred into a
611 T25 flask. The cells recovered for at least 30 mins at room temperature by gentle
612 shaking (50 rpm). Following recovery, the cells were centrifuged (200 × g for 1.5
613 minutes) and resuspended in extracellular buffer (10 mM HEPES, 145 mM NaCl, 4 mM
614 KCl, 1 mM MgCl₂, 2 mM CaCl₂, 10 mM glucose, pH 7.4) to a cell density of 3-7 × 10⁶
615 cells/mL. The osmolality of the extracellular buffer was adjusted using a Vapro 5600
616 vapor pressure osmometer (Wescor) with sucrose to 315-330 mOSm and pH using
617 NaOH.

618 Data was collected using IonFluxMercury HT (Cell Microsystems) automated
619 patch clamp electrophysiology instrument with Ionflux HT v5.0 software using ensemble
620 IonFlux Plate HT (Cell Microsystems 910-0055). The ensemble microfluidic plates
621 enable 32 parallel experiments with aggregate currents from 20 cells per experiment.
622 Intracellular solution was composed of 10 mM HEPES, 120 mM KCl, 1.75 mM MgCl₂,
623 5.374 mM CaCl₂, 10 mM EGTA, 4 mM NaATP, pH 7.2. The intracellular solution
624 osmolality was adjusted with sucrose to 305-315 mOsm and the pH was adjusted using
625 KOH. Class I or II compounds were dissolved into DMSO before adding to extracellular
626 solution, where the DMSO concentration was kept consistent at 0.03% v/v across all
627 compounds and controls. Prior to experiments the plates were washed as suggested by

628 the manufacturer. The protocol for the experiment is divided into four steps: prime
629 (priming microfluidics with solutions), trap (trap cells and obtain membrane seals), break
630 (access to intracellular by breaking membrane), and data acquisition. Each step also
631 has multiple channels: main channel (positive pressure allows solutions to flow towards
632 the cells and waste), trap channel (negative pressure to provide a vacuum to keep the
633 cells in the traps and break the cell membrane to access intracellular), and compound
634 channel (positive pressure to flow compounds to main channel). During the prime step:
635 (1) the main channel was applied 1 psi for $t = 0-25$ s and 0.4 psi for $t = 25-60$ s (2) the
636 trap and compound channels were applied at 5 psi for $t = 0-20$ s and then 1.5 psi for $t =$
637 $20-55$ s followed by only the traps at 2 psi for $t = 55-60$ s. For the voltage during the
638 prime step, a pulse was applied every 150 ms, where the 0 mV holding potential was
639 applied during $t = 0-50$ ms, 20 mV was applied during the $t = 50-100$ ms, and 0 mV
640 during the $t = 100-150$ ms. During the trap step: (1) the main channel is applied 0.1 psi
641 for $t = 0-5$ s before applying 0.5 s pulses of 0.2 psi every 5 s during $t = 5-135$ s (2) the
642 trap channel is applied 6 inHg for $t = 0-135$ s. For the voltage during the trap step, a
643 pulse was applied every 70 ms, where the -80 mV holding potential was applied
644 between $t = 0-20$ ms, -100 mV for $t = 20-50$ ms, -80 mV for $t = 50-70$ ms. During the
645 break step: (1) the main channel is applied 0.1 psi for $t = 0-100$ s (2) the trap channel
646 was applied 6 inHg between $t = 0-10$ s, vacuum ramp from 10 to 14 inHg from $t = 10-40$
647 s, and 6 inHg for $t = 40-100$ s. For the voltage during the break step, a pulse was
648 applied every 150 ms, where -80 mV holding potential was applied between $t = 0-50$
649 ms, -100 mV for $t = 50-100$ ms, and -80 mV for $t = 100-150$ ms. During the data
650 acquisition: (1) the main channel is applied at 0.15 psi for $t = 0-1350$ s and 0 psi for

651 1350-2450 s, (2) the traps channel is applied 5 inHg for t = 0-3 s, 3 inHg for t = 3-1350
652 s, and 0 inHG for t = 1350-2450 s. For the voltage during the data acquisition, a pulse
653 was applied every 625 ms, where the -60 mV holding potential was applied between t =
654 0-100 ms, -70 mV for t = 100-200 ms, -60 mV for t = 200-300 ms, a voltage ramp from -
655 120 mV to 160 mV for t = 300-525 ms and -60 mV for t = 525-625 ms. The cells/plates
656 were equilibrated to 30 °C for 5 minutes. Prior to application of a Class I or Class II
657 compound, menthol was perfused for 75 s four times to measure initial current
658 responses. Compounds were then applied by continuous perfusion for 15 minutes
659 followed by measurement of two 75 s applications of menthol in in the presence of
660 compound.

661 Ionflux Data Analyzer v5.0 was used to analyze the data. Leak subtraction was
662 performed on the data based on the -60 mV initial holding potential and -70 mV voltage
663 steps from the data acquisition. Each point of the current trace is from the difference of
664 the current at 120 mV and the holding potential at -60 mV. The data was averaged from
665 7 points after 25 s of perfusion of menthol without or with the compound. The last two
666 menthol stimulated currents before compound application were averaged and compared
667 to the two menthol-stimulated currents after compound application to determine a ratio
668 of menthol response.

669

670 **TRPM8 cell surface measurements**

671 TRPM8 stable cells were cultured as described above. Cells were collected by
672 dissociation with 0.5 mM EDTA in PBS and resuspended in media. Cells were then
673 incubated in 100 µl of media with 10 µM compound or 10 mM MBCD for 15 minutes as

674 in the electrophysiology experiments. Cells were then fixed with 100 μ l Buffer A from a
675 Fix & Perm kit for flow cytometry (Invitrogen, Cat. No. GAS004). Cells were then rinsed
676 3 times in flow cytometry buffer (PBS + 5% FBS + 0.1% NaN₃). Cells were then labeled
677 with either of two TRPM8 primary antibodies targeted to an extracellular epitope
678 (Alomone, Cat. No. ACC-049 Abcepta, Cat. No. AP8181D). The Alomone antibody was
679 used at a dilution of 1:100 while the Abcepta antibody was used at a dilution of 1:50 for
680 1 hr in the flow cytometry buffer. Cells were rinsed 3 times again then labeled with an
681 anti-Rabbit-AlexaFlour488 secondary at a 1:1000 dilution (Cell Signaling, Cat. No.
682 4412) for 45 min. Cells were rinsed 3 \times again and resuspended in a final volume of 300
683 μ l. Single cell fluorescence intensities were measured on a BD Fortessa 5-laser
684 analytical cytometer. Geometric means of the resulting intensity distributions were
685 calculated in FlowJo (version 10). Statistical comparisons were made in GraphPad
686 Prism (version 10).

687

688 **Immunoblotting to detect EGFR activation**

689 For EGFR activation studies, adherent HeLa cells at 70 % confluency in a 60 mm dish
690 were starved overnight (~18 hr) with starvation media - serum free DMEM/F12 (Gibco)
691 media supplemented with only Pen-Step. Starved cells were exposed to small
692 molecules of interest by replacing the overnight starvation media with 4 mL of pre-
693 warmed starvation media containing 10 μ M of Class I or II molecule of interest and 0.1
694 % DMSO (Cell Signaling Technologies) for noted times at 37 °C. After incubation,
695 EGFR was activated with the addition of 1 mL of pre-warmed starvation media
696 containing 500 ng/mL EGF (R&D Systems) for 1 minute. Due to the speed of EGFR

697 activation kinetics in HeLa cells, treated plates were then flash frozen in liquid nitrogen
698 after media removal. Frozen plates were then placed on ice and lysed with scraping in
699 ice-cold RIPA lysis buffer supplemented with PhosStop phosphatase inhibitor and
700 Complete protease inhibitor (Roche). Lysates were clarified by centrifugation and
701 subjected to immunoblotting using NuPage Novex 4 % - 12 % Bis-Tris Protein Gels
702 (ThermoFisher Scientific). After electrophoresis, intact gels were transferred to
703 Immobilon-P PVDF (Millipore) membranes and cut into three horizontal strips guided by
704 Precision Plus molecular weight ladder (Bio-Rad) and incubated overnight in blocking
705 buffer - 20 mM Tris, 150 mM NaCl, 0.1 % Tween-20 (Bio-Rad) pH 7.6 (TBST) with 3 %
706 w/v Bovine Serum Albumin Fraction V (Fisher Bioreagents). Primary rabbit antibodies
707 against EGFR pY1173 (53A5, 3972S), phospho-p44/42 MAPK – also known as ERK
708 1/2 (9101S), and GRB2 (3972S) were purchased from Cell Signaling Technology and
709 used at a dilution of 1:1000 in TBST for 1 hr at RT with gentle agitation. Goat anti-rabbit
710 IgG (H+L) conjugated to horse radish peroxidase (ThermoFisher Scientific, 31460) with
711 glycerol was used at a dilution of 1:5000 for 1 hr in blocking buffer with gentle agitation.
712 Blots were detected using SuperSignal West Pico Chemiluminescent Substrate
713 (ThermoFisher Scientific) on a LI-COR 2800 using the chemiluminescent and 700 nm
714 channels to detect antibody and molecular weight bands signals, respectively.
715 Chemiluminescent signal was checked for saturation and bands of interest were
716 integrated with Image Studio (LI-COR, version 3.1).

717 References

- 718
- 719 1. Heberle, F. A., and Feigenson, G. W. (2011) Phase Separation in Lipid Membranes. *Cold Spring Harb*
720 *Perspect Biol.* **3**, a004630
- 721 2. Veatch, S. L., Rogers, N., Decker, A., and Shelby, S. A. (2023) The plasma membrane as an adaptable fluid
722 mosaic. *Biochimica et Biophysica Acta (BBA) - Biomembranes.* **1865**, 184114
- 723 3. Shaw, T. R., Ghosh, S., and Veatch, S. L. (2020) Critical Phenomena in Plasma Membrane Organization
724 and Function. *Annu Rev Phys Chem.* **72**, 51
- 725 4. Rayermann, S. P., Rayermann, G. E., Cornell, C. E., Merz, A. J., and Keller, S. L. (2017) Hallmarks of
726 Reversible Separation of Living, Unperturbed Cell Membranes into Two Liquid Phases. *Biophys J.* **113**,
727 2425–2432
- 728 5. Lingwood, D., and Simons, K. (2010) Lipid rafts as a membrane-organizing principle. *Science (1979).* **327**,
729 46–50
- 730 6. Staubach, S., and Hanisch, F. G. (2011) Lipid rafts: signaling and sorting platforms of cells and their roles in
731 cancer. *Expert Rev Proteomics.* **8**, 263–277
- 732 7. Tsui-Pierchala, B. A., Encinas, M., Milbrandt, J., and Johnson, E. M. (2002) Lipid rafts in neuronal
733 signaling and function. *Trends Neurosci.* **25**, 412–417
- 734 8. Mollinedo, F., and Gajate, C. (2020) Lipid rafts as signaling hubs in cancer cell survival/death and invasion:
735 Implications in tumor progression and therapy. *J Lipid Res.* **61**, 611–635
- 736 9. Roy, A., and Patra, S. K. (2022) Lipid Raft Facilitated Receptor Organization and Signaling: A Functional
737 Rheostat in Embryonic Development, Stem Cell Biology and Cancer. *Stem Cell Reviews and Reports 2022*
738 *19:1.* **19**, 2–25
- 739 10. Brown, D. A., and London, E. (1998) Functions of lipid rafts in biological membranes. *Annu Rev Cell Dev*
740 *Biol.* **14**, 111–136
- 741 11. Varshney, P., Yadav, V., and Saini, N. (2016) Lipid rafts in immune signalling: current progress and future
742 perspective. *Immunology.* **149**, 13–24
- 743 12. Viljetic, B., Blažetić, S., Labak, I., Ivić, V., Zjalić, M., Heffer, M., and Balog, M. (2024) Lipid Rafts: The
744 Maestros of Normal Brain Development. *Biomolecules 2024, Vol. 14, Page 362.* **14**, 362
- 745 13. Mañes, S., Del Real, G., and Martínez-A, C. (2003) Pathogens: raft hijackers. *Nature Reviews Immunology*
746 *2003 3:7.* **3**, 557–568
- 747 14. Parton, R. G., and Richards, A. A. (2003) Lipid Rafts and Caveolae as Portals for Endocytosis: New Insights
748 and Common Mechanisms. *Traffic.* **4**, 724–738
- 749 15. Head, B. P., Patel, H. H., and Insel, P. A. (2014) Interaction of membrane/lipid rafts with the cytoskeleton:
750 Impact on signaling and function: Membrane/lipid rafts, mediators of cytoskeletal arrangement and cell
751 signaling. *Biochimica et Biophysica Acta (BBA) - Biomembranes.* **1838**, 532–545
- 752 16. Pralle, A., Keller, P., Florin, E. L., Simons, K., and Hörber, J. K. H. (2000) Sphingolipid–Cholesterol Rafts
753 Diffuse as Small Entities in the Plasma Membrane of Mammalian Cells. *Journal of Cell Biology.* **148**, 997–
754 1008
- 755 17. Bolmatov, D., Soloviov, D., Zhernenkov, M., Zav'Yalov, D., Mamontov, E., Suvorov, A., Cai, Y. Q., and
756 Katsaras, J. (2020) Molecular Picture of the Transient Nature of Lipid Rafts. *Langmuir.* **36**, 4887–4896
- 757 18. Janosi, L., Li, Z., Hancock, J. F., and Gorfé, A. A. (2012) Organization, dynamics, and segregation of Ras
758 nanoclusters in membrane domains. *Proc Natl Acad Sci U S A.* **109**, 8097–8102
- 759 19. Sezgin, E., Kaiser, H. J., Baumgart, T., Schwille, P., Simons, K., and Levental, I. (2012) Elucidating
760 membrane structure and protein behavior using giant plasma membrane vesicles. *Nat Protoc.* **7**, 1042–1051
- 761 20. Fridriksson, E. K., Shipkova, P. A., Sheets, E. D., Holowka, D., Baird, B., and McLafferty, F. W. (1999)
762 Quantitative analysis of phospholipids in functionally important membrane domains from RBL-2H3 mast
763 cells using tandem high-resolution mass spectrometry. *Biochemistry.* **38**, 8056–8063
- 764 21. Bauer, B., Davidson, M., and Orwar, O. (2009) Proteomic Analysis of Plasma Membrane Vesicles.
765 *Angewandte Chemie.* **121**, 1684–1687
- 766 22. Lorent, J. H., Diaz-Rohrer, B., Lin, X., Spring, K., Gorfé, A. A., Levental, K. R., and Levental, I. (2017)
767 Structural determinants and functional consequences of protein affinity for membrane rafts. *Nature*
768 *Communications 2017 8:1.* **8**, 1–10
- 769 23. Castello-Serrano, I., Lorent, J. H., Ippolito, R., Levental, K. R., and Levental, I. (2020) Myelin-Associated
770 MAL and PLP Are Unusual among Multipass Transmembrane Proteins in Preferring Ordered Membrane
771 Domains. *J Phys Chem B.* **124**, 5930–5939

- 772 24. Levental, I., Lingwood, D., Grzybek, M., Coskun, Ü., and Simons, K. (2010) Palmitoylation regulates raft
773 affinity for the majority of integral raft proteins. *Proc Natl Acad Sci U S A.* **107**, 22050–22054
- 774 25. Marinko, J. T., Kenworthy, A. K., and Sanders, C. R. (2020) Peripheral myelin protein 22 preferentially
775 partitions into ordered phase membrane domains. *Proceedings of the National Academy of Sciences.* **117**,
776 14168–14177
- 777 26. Divincenzo, C., Elzinga, C. D., Medeiros, A. C., Karbassi, I., Jones, J. R., Evans, M. C., Braastad, C. D.,
778 Bishop, C. M., Jaremko, M., Wang, Z., Liaquat, K., Hoffman, C. A., York, M. D., Batish, S. D., Lupski, J.
779 R., and Higgins, J. J. (2014) The allelic spectrum of charcot–marie–tooth disease in over 17,000 individuals
780 with neuropathy. *Mol Genet Genomic Med.* **2**, 522–529
- 781 27. Li, J., Parker, B., Martyn, C., Natarajan, C., Guo, J., Li, J., Parker, : B, Martyn, : C, Natarajan, C., and Guo,
782 J. (2012) The PMP22 Gene and Its Related Diseases. *Molecular Neurobiology* 2012 47:2. **47**, 673–698
- 783 28. Schleich, J. P., Narayan, M., Alford, C., Mittendorf, K. F., Carter, B. D., Li, J., and Sanders, C. R. (2015)
784 Conformational Stability and Pathogenic Misfolding of the Integral Membrane Protein PMP22. *J Am Chem*
785 *Soc.* **137**, 8758–8768
- 786 29. Stefanski, K. M., Wilkinson, M. C., and Sanders, C. R. (2024) Roles for PMP22 in Schwann cell cholesterol
787 homeostasis in health and disease. *Biochem Soc Trans.* **52**, 1747–1756
- 788 30. Fricke, N., Raghunathan, K., Tiwari, A., Stefanski, K. M., Balakrishnan, M., Waterson, A. G., Capone, R.,
789 Huang, H., Sanders, C. R., Bauer, J. A., and Kenworthy, A. K. (2022) High-Content Imaging Platform to
790 Discover Chemical Modulators of Plasma Membrane Rafts. *ACS Cent Sci.* **8**, 370–378
- 791 31. Marinko, J. T., Wright, M. T., Schleich, J. P., Clowes, K. R., Heintzman, D. R., Plate, L., and Sanders, C.
792 R. (2021) Glycosylation limits forward trafficking of the tetraspan membrane protein PMP22. *Journal of*
793 *Biological Chemistry.* 10.1016/j.jbc.2021.100719
- 794 32. Zhang, X. D. (2010) Strictly Standardized Mean Difference, Standardized Mean Difference and Classical t-
795 test for the Comparison of Two Groups. *Stat Biopharm Res.* **2**, 292–299
- 796 33. Skinkle, A. D., Levental, K. R., and Levental, I. (2020) Cell-Derived Plasma Membrane Vesicles Are
797 Permeable to Hydrophilic Macromolecules. *Biophys J.* **118**, 1292–1300
- 798 34. Bajusz, D., Rácz, A., and Héberger, K. (2015) Why is Tanimoto index an appropriate choice for fingerprint-
799 based similarity calculations? *J Cheminform.* **7**, 1–13
- 800 35. Jin, L., Millard, A. C., Wuskell, J. P., Dong, X., Wu, D., Clark, H. A., and Loew, L. M. (2006)
801 Characterization and Application of a New Optical Probe for Membrane Lipid Domains. *Biophys J.* **90**,
802 2563–2575
- 803 36. Peier, A. M., Moqrich, A., Hergarden, A. C., Reeve, A. J., Andersson, D. A., Story, G. M., Earley, T. J.,
804 Dragoni, I., McIntyre, P., Bevan, S., and Patapoutian, A. (2002) A TRP Channel that Senses Cold Stimuli
805 and Menthol. *Cell.* **108**, 705–715
- 806 37. McKemy, D. D., Neuhauser, W. M., and Julius, D. (2002) Identification of a cold receptor reveals a general
807 role for TRP channels in thermosensation. *Nature* 2002 416:6876. **416**, 52–58
- 808 38. Martens, J. R., O’Connell, K., and Tamkun, M. (2004) Targeting of ion channels to membrane
809 microdomains: Localization of K⁺ V channels to lipid rafts. *Trends Pharmacol Sci.* **25**, 16–21
- 810 39. Bobkov, D., and Semenova, S. (2022) Impact of lipid rafts on transient receptor potential channel activities.
811 *J Cell Physiol.* **237**, 2034–2044
- 812 40. Kimchi, O., Veatch, S. L., and Machta, B. B. (2018) Ion channels can be allosterically regulated by
813 membrane domains near a de-mixing critical point. *Journal of General Physiology.* **150**, 1769–1777
- 814 41. Morenilla-Palao, C., Pertusa, M., Meseguer, V., Cabedo, H., and Viana, F. (2009) Lipid Raft Segregation
815 Modulates TRPM8 Channel Activity. *Journal of Biological Chemistry.* **284**, 9215–9224
- 816 42. Dutta, D., and Donaldson, J. G. (2012) Search for inhibitors of endocytosis. *Cell Logist.* **2**, 203–208
- 817 43. Lambert, S., Vind-Kezunovic, D., Karvinen, S., and Gniadecki, R. (2006) Ligand-Independent Activation of
818 the EGFR by Lipid Raft Disruption. *Journal of Investigative Dermatology.* **126**, 954–962
- 819 44. Irwin, M. E., Mueller, K. L., Bohin, N., Ge, Y., and Boerner, J. L. (2011) Lipid raft localization of EGFR
820 alters the response of cancer cells to the EGFR tyrosine kinase inhibitor gefitinib. *J Cell Physiol.* **226**, 2316–
821 2328
- 822 45. Chen, X., and Resh, M. D. (2002) Cholesterol Depletion from the Plasma Membrane Triggers Ligand-
823 independent Activation of the Epidermal Growth Factor Receptor. *Journal of Biological Chemistry.* **277**,
824 49631–49637
- 825 46. Machta, B. B., Gray, E., Nouri, M., McCarthy, N. L. C., Gray, E. M., Miller, A. L., Brooks, N. J., and
826 Veatch, S. L. (2016) Conditions that Stabilize Membrane Domains Also Antagonize n-Alcohol Anesthesia.
827 *Biophys J.* **111**, 537–545

- 828 47. Mahammad, S., and Parmryd, I. (2015) Cholesterol depletion using methyl- β -cyclodextrin. *Methods Mol Biol.* **1232**, 91–102
- 829
- 830 48. Suresh, P., and London, E. (2022) Using cyclodextrin-induced lipid substitution to study membrane lipid and ordered membrane domain (raft) function in cells. *Biochimica et Biophysica Acta (BBA) - Biomembranes.* **1864**, 183774
- 831
- 832
- 833 49. Morenilla-Palao, C., Pertusa, M., Meseguer, V., Cabedo, H., and Viana, F. (2009) Lipid raft segregation modulates TRPM8 channel activity. *Journal of Biological Chemistry.* **284**, 9215–9224
- 834
- 835 50. Veliz, L. A., Toro, C. A., Vivar, J. P., Arias, L. A., Villegas, J., Castro, M. A., and Brauchi, S. (2010) Near-Membrane Dynamics and Capture of TRPM8 Channels within Transient Confinement Domains. *PLoS One.* **5**, e13290
- 836
- 837
- 838 51. Hilton, J. K., Salehpour, T., Sisco, N. J., Rath, P., and Van Horn, W. D. (2018) Phosphoinositide-interacting regulator of TRP (PIRT) has opposing effects on human and mouse TRPM8 ion channels. *Journal of Biological Chemistry.* **293**, 9423–9434
- 839
- 840
- 841 52. Journigan, V. B., Alarcón-Alarcón, D., Feng, Z., Wang, Y., Liang, T., Dawley, D. C., Amin, A. R. M. R., Montano, C., Van Horn, W. D., Xie, X. Q., Ferrer-Montiel, A., and Fernández-Carvajal, A. (2021) Structural and in Vitro Functional Characterization of a Menthyl TRPM8 Antagonist Indicates Species-Dependent Regulation. *ACS Med Chem Lett.* **12**, 758–767
- 842
- 843
- 844
- 845 53. Hilton, J. K., Rath, P., Helsell, C. V. M., Beckstein, O., and Van Horn, W. D. (2015) Understanding thermosensitive transient receptor potential channels as versatile polymodal cellular sensors. *Biochemistry.* **54**, 2401–2413
- 846
- 847
- 848 54. Garami, A., Shimansky, Y. P., Rumbus, Z., Vizin, R. C. L., Farkas, N., Hegyi, J., Szakacs, Z., Solymar, M., Csenkey, A., Chiche, D. A., Kapil, R., Kyle, D. J., Van Horn, W. D., Hegyi, P., and Romanovsky, A. A. (2020) Hyperthermia induced by transient receptor potential vanilloid-1 (TRPV1) antagonists in human clinical trials: Insights from mathematical modeling and meta-analysis. *Pharmacol Ther.* **208**, 107474
- 849
- 850
- 851
- 852 55. Ruzzi, F., Cappello, C., Semprini, M. S., Scalambra, L., Angelicola, S., Pittino, O. M., Landuzzi, L., Palladini, A., Nanni, P., and Lollini, P. L. (2024) Lipid rafts, caveolae, and epidermal growth factor receptor family: friends or foes? *Cell Commun Signal.* **22**, 489
- 853
- 854
- 855 56. Jakubík, J., and El-Fakahany, E. E. (2021) Allosteric Modulation of GPCRs of Class A by Cholesterol. *International Journal of Molecular Sciences 2021, Vol. 22, Page 1953.* **22**, 1953
- 856
- 857 57. Ballweg, S., Sezgin, E., Doktorova, M., Covino, R., Reinhard, J., Wunnicke, D., Hänel, I., Levental, I., Hummer, G., and Ernst, R. (2020) Regulation of lipid saturation without sensing membrane fluidity. *Nature Communications 2020 11:1.* **11**, 1–13
- 858
- 859
- 860 58. Levental, I., Levental, K. R., and Heberle, F. A. (2020) Lipid Rafts: Controversies Resolved, Mysteries Remain. *Trends Cell Biol.* **30**, 341–353
- 861
- 862 59. Kervin, T. A., and Overduin, M. (2024) Membranes are functionalized by a proteolipid code. *BMC Biol.* **22**, 1–7
- 863
- 864 60. Levental, K. R., Lorent, J. H., Lin, X., Skinkle, A. D., Surma, M. A., Stockenbojer, E. A., Gorfe, A. A., and Levental, I. (2016) Polyunsaturated Lipids Regulate Membrane Domain Stability by Tuning Membrane Order. *Biophys J.* **110**, 1800–1810
- 865
- 866
- 867 61. Mason, R. P., Jacob, R. F., Shrivastava, S., Sherratt, S. C. R., and Chattopadhyay, A. (2016) Eicosapentaenoic acid reduces membrane fluidity, inhibits cholesterol domain formation, and normalizes bilayer width in atherosclerotic-like model membranes. *Biochimica et Biophysica Acta (BBA) - Biomembranes.* **1858**, 3131–3140
- 868
- 869
- 870
- 871 62. Ernst, R., Ejsing, C. S., and Antonny, B. (2016) Homeoviscous Adaptation and the Regulation of Membrane Lipids. *J Mol Biol.* **428**, 4776–4791
- 872
- 873 63. Renne, M. F., and Ernst, R. (2023) Membrane homeostasis beyond fluidity: control of membrane compressibility. *Trends Biochem Sci.* **48**, 963–977
- 874
- 875 64. Hazel, J. R. (1995) THERMAL ADAPTATION IN BIOLOGICAL MEMBRANES: Is Homeoviscous Adaptation the Explanation? *AmlU. Rev. Physiol.* **57**, 19–42
- 876
- 877 65. Veatch, S. L., Cicuta, P., Sengupta, P., Honerkamp-Smith, A., Holowka, D., and Baird, B. (2008) Critical fluctuations in plasma membrane vesicles. *ACS Chem Biol.* **3**, 287–293
- 878
- 879 66. Zhang, X. D., Ferrer, M., Espeseth, A. S., Marine, S. D., Stec, E. M., Crackower, M. A., Holder, D. J., Heyse, J. F., and Strulovici, B. (2007) The Use of Strictly Standardized Mean Difference for Hit Selection in Primary RNA Interference High-Throughput Screening Experiments. <http://dx.doi.org/10.1177/1087057107300646>. **12**, 497–509
- 880
- 881
- 882

- 883 67. Dharan, R., Goren, S., Cheppali, S. K., Shendrik, P., Brand, G., Vaknin, A., Yu, L., Kozlov, M. M., and
884 Sorkin, R. (2022) Transmembrane proteins tetraspanin 4 and CD9 sense membrane curvature. *Proc Natl*
885 *Acad Sci U S A*. **119**, e2208993119
- 886 68. Schindelin, J., Arganda-Carreras, I., Frise, E., Kaynig, V., Longair, M., Pietzsch, T., Preibisch, S., Rueden,
887 C., Saalfeld, S., Schmid, B., Tinevez, J. Y., White, D. J., Hartenstein, V., Eliceiri, K., Tomancak, P., and
888 Cardona, A. (2012) Fiji: an open-source platform for biological-image analysis. *Nature Methods* **2012** 9:7.
889 **9**, 676–682
- 890 69. Strober, W. (1997) Trypan Blue Exclusion Test of Cell Viability. *Curr Protoc Immunol*. **21**, A.3B.1-A.3B.2
- 891 70. Luu, D. D., Ramesh, N., Can Kazan, I., Shah, K. H., Lahiri, G., Mana, M. D., Banu Ozkan, S., and Van
892 Horn, W. D. (2024) Evidence that the cold- and menthol-sensing functions of the human TRPM8 channel
893 evolved separately. *Sci Adv*. **10**, 9228
- 894

895 **Acknowledgments**

896
897 The MAL-GFP construct was a gift from the Levental lab (University of Virginia).
898 Some experiments were performed in the Vanderbilt High-Throughput Screening
899 (HTS) Core Facility with assistance provided by Corbin Whitwell. The FDA
900 approved library was provided by the Vanderbilt CTSA and distributed by the
901 Vanderbilt High-Throughput Screening Core Facility as was the Vanderbilt
902 Discovery Collection. The HTS Core receives support from the Vanderbilt
903 Institute of Chemical Biology and the Vanderbilt Ingram Cancer Center.
904 Membrane fluidity experiments were performed in part through the use of the
905 Vanderbilt Cell Imaging Shared Resource.

906 **Funding:**

907
908 National Institutes of Health grant R01 GM138493 (AKK, CRS)
909 National Institutes of Health grant R01 NS095989 (CRS)
910 National Institutes of Health grant R35 GM141933 (WDVH)
911 National Institutes of Health grant F32 GM151766 (JMH)
912 National Institutes of Health grant 1S10OD021630
913 National Institutes of Health grant CA68485
914 National Institutes of Health grant DK20593
915 National Institutes of Health grant DK58404
916 National Institutes of Health grant DK59637
917 National Institutes of Health grant EY08126
918 National Institutes of Health grant P30 CA68485
919 National Institutes of Health grant UL1TR00044
920 CMT Research Foundation grant (CRS)

921 **Author contributions:**

922
923
924 Conceptualization: KMS, AKK, WDHV, CRS
925 Methodology: KMS, HH, JAB, AKK, WDVH, CRS
926 Investigation: KMS, HH, DDL, JMH, NS, AJF, TPH
927 Supervision: JAB, AKK, WDVH, CRS
928 Writing—original draft: KMS, CRS
929 Writing—review & editing: KMS, HH, DDL, JAB, AKK, WDVH, CRS

930

931 **Competing interests:** Authors declare that they have no competing interests.

932

933 **Data and materials availability:** All data are available in the main text or the
934 supplementary materials.

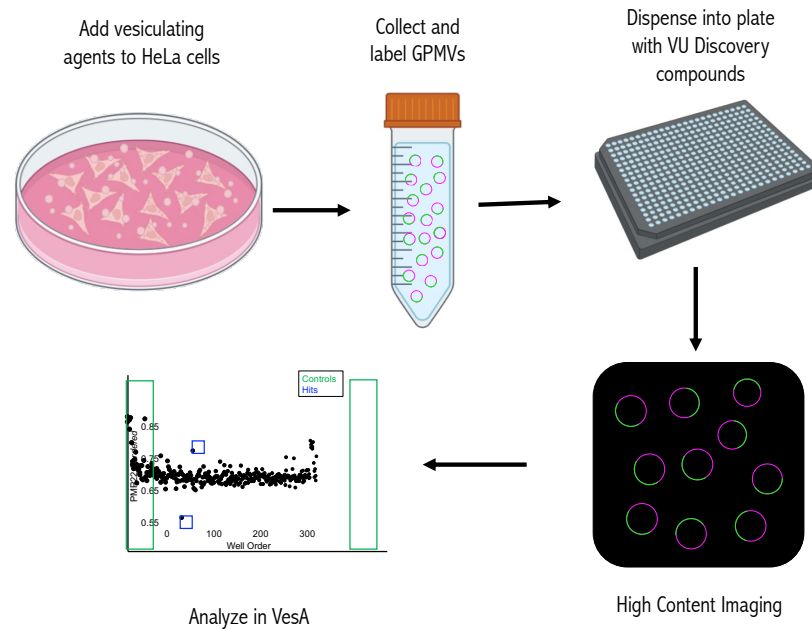


Figure 1. High-throughput screening approach to identify modulators of PMP22 raft affinity. Pipeline used to screen 24,000+ compounds that identified hits described here.

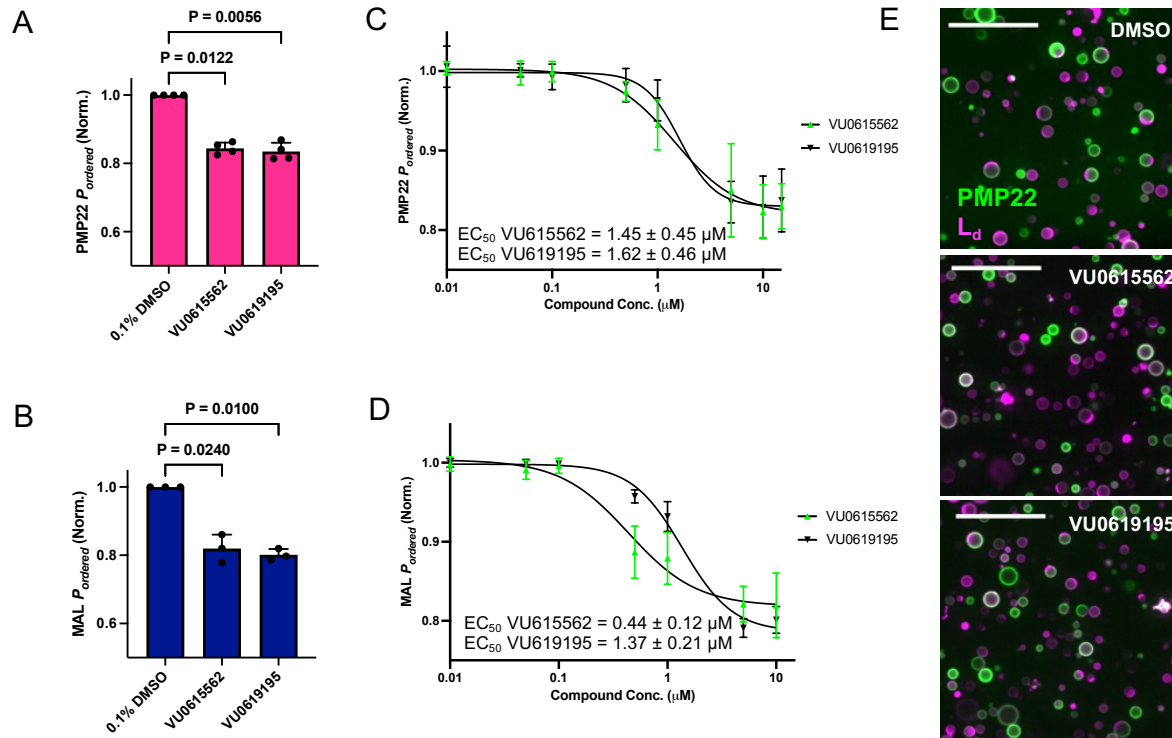


Figure 2. Class I modulators affect the affinity of PMP22 and MAL for ordered domains. A) Hit compounds VU0615562 and VU0619195 decrease ordered partitioning of PMP22 ($n = 4$) and **B)** MAL ($n = 3$) at 10 μ M. Bars are means \pm SD. P-values are from Mann-Whitney tests. **C)** Dose-response experiments determined EC_{50} for the impact of VU0615562 and VU0619195 on PMP22 ordered partitioning and **D)** MAL ordered partitioning. Points are mean \pm SD, $n = 3$. Curves and EC_{50} values are from non-linear, sigmoidal fits, \pm SE. **E)** Representative images of GPMVs treated with 0.5 μ M compound. Scale bars are 50 μ m.

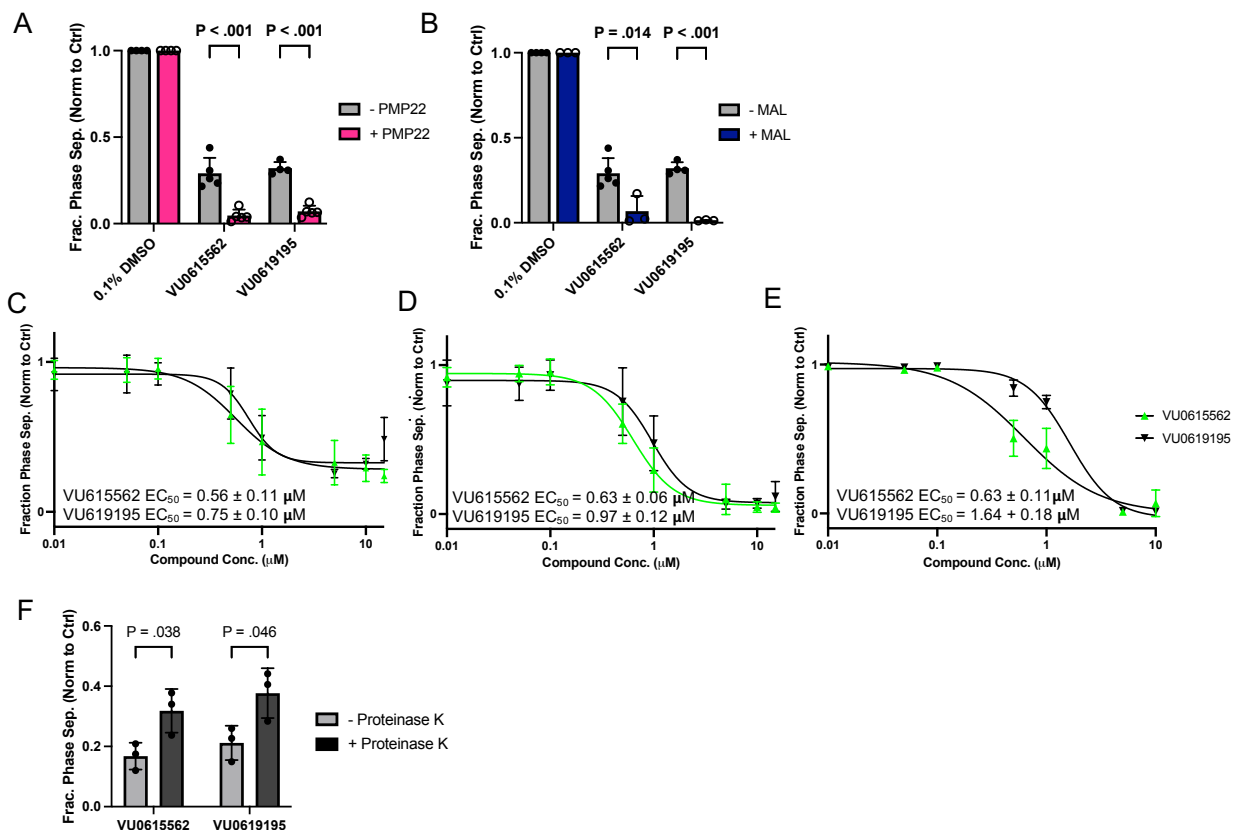


Figure 3. Class I compounds decrease raft formation in a protein-dependent manner. A) Effects of 10 μ M VU0615562 and VU0619195 on the fraction of phase separated GPMVs with PMP22 expression (magenta bars) or from untransfected cells (gray bars) ($n = 4-5$). **B)** Effects of VU0615562 and VU0619195 on the fraction of phase separated GPMVs with MAL expression (navy bars) or from untransfected cells (gray bars) expression 10 μ M ($n = 3-5$). **The middle three panels present dose response experiments** used to determine EC_{50} values of compounds on phase separation in GPMVs from **C)** cells not expressing PMP22 or MAL, **D)** cells expressing PMP22, and **E)** cells expressing MAL. $n = 3$, points are means \pm SD. Curves and EC_{50} values \pm SE are from non-linear, sigmoidal fits. **F)** Effects of 10 μ M compounds on the fraction of phase separated GPMVs with (dark gray bars) and without proteinase K treatment from untransfected cells ($n = 3$). Bars are means \pm SD. P-values are from unpaired student's t-tests.

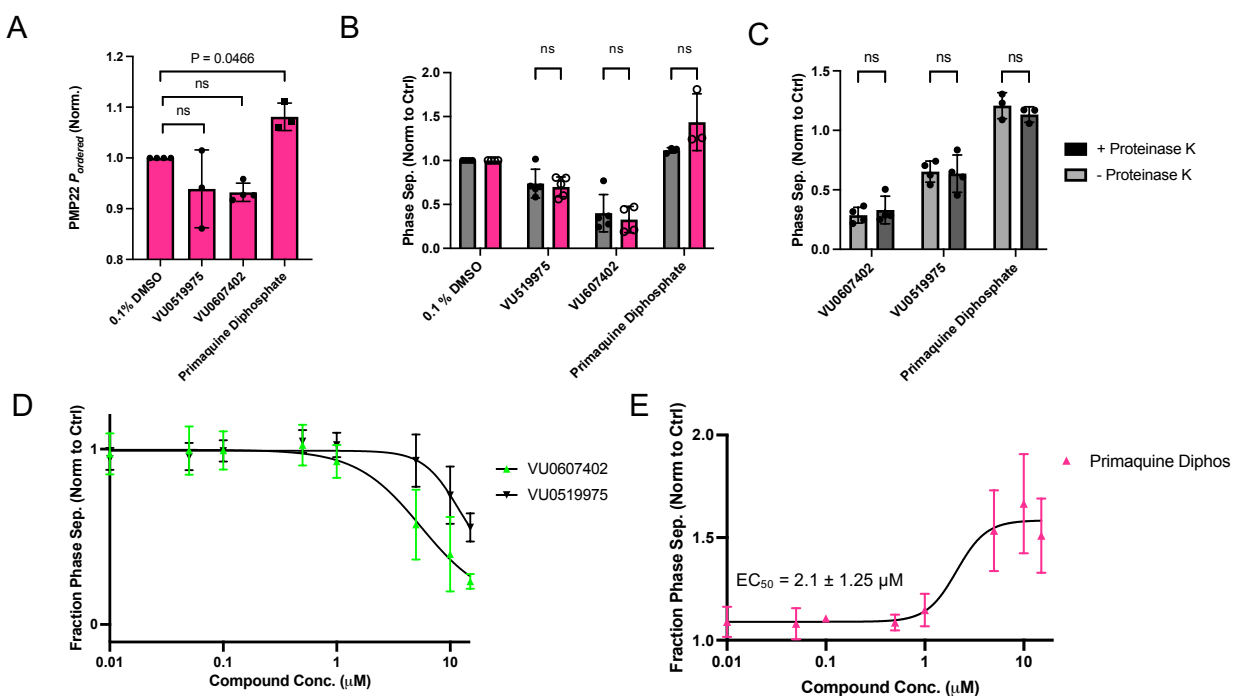


Figure 4. Screening identified raft modulators that are protein-independent. **A)** Effects of 10 μM VU0519975, VU06107402, and primaquine diphosphate on ordered partitioning of PMP22. Bars are means \pm SD ($n = 3$), p-values are from Dunnett's test. **B)** Effects of 10 μM VU0519975, VU06107402, and primaquine diphosphate on raft formation in GPMVs with PMP22 (magenta bars) or from untransfected cells (gray bars) PMP22 expression. Bars are means \pm SD ($n = 3-5$) **C)** Effects of 10 μM VU0519975, VU06107402, and primaquine diphosphate on GPMV phase separation with (dark gray bars) and without (gray bars) proteinase K treatment **from untransfected cells** ($n = 3-5$). **D)** Dose response experiments with VU0519975 and VU06107402 ($n = 3$). **E)** Dose response experiments with primaquine diphosphate on raft formation. Points are means \pm SD ($n = 3$). Curve and EC_{50} value from non-linear, sigmoidal fits \pm SE.

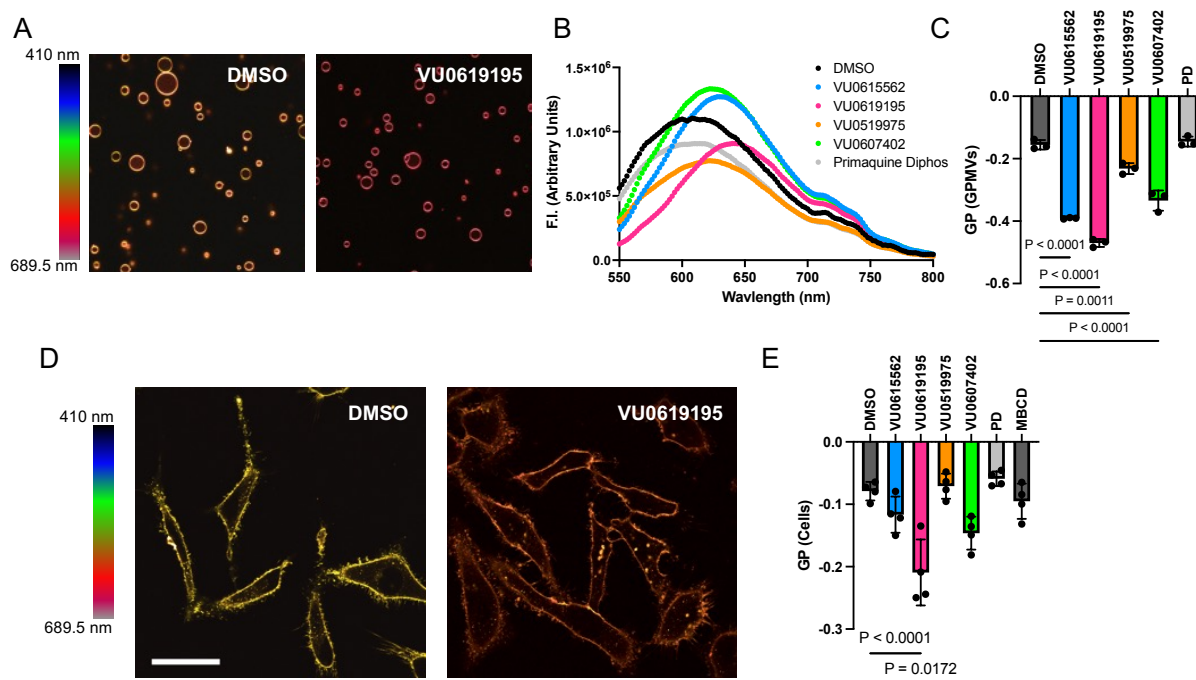


Figure 5. Compounds alter membrane fluidity in GPMVs and live cells. A) Representative spectral images (cropped from 40X fields) of GPMVs stained with Di-4 and treated with DMSO or 10 μ M VU0619195. **B)** Representative Di-4 emission spectra of GPMVs treated with 10 μ M hit compounds. **C)** Generalized polarization values calculated from Di-4 emission spectra shown in B. Bars are means \pm SD ($n = 3$). P-values are from ANOVA followed by Dunnett's multiple comparisons tests. **D)** Representative spectral images of live HeLa cells stained with Di-4 and treated with DMSO or 10 μ M VU0619195. Scale bar = 50 μ m. **E)** Generalized polarization values calculated from Di-4 emission intensities calculated from individual cells as shown in D. Bars are means \pm SD, 10-15 cells (technical replicates) per treatment were measured for each of 4 biological replicates. P-values are from ANOVA followed by Dunnett's multiple comparisons tests.

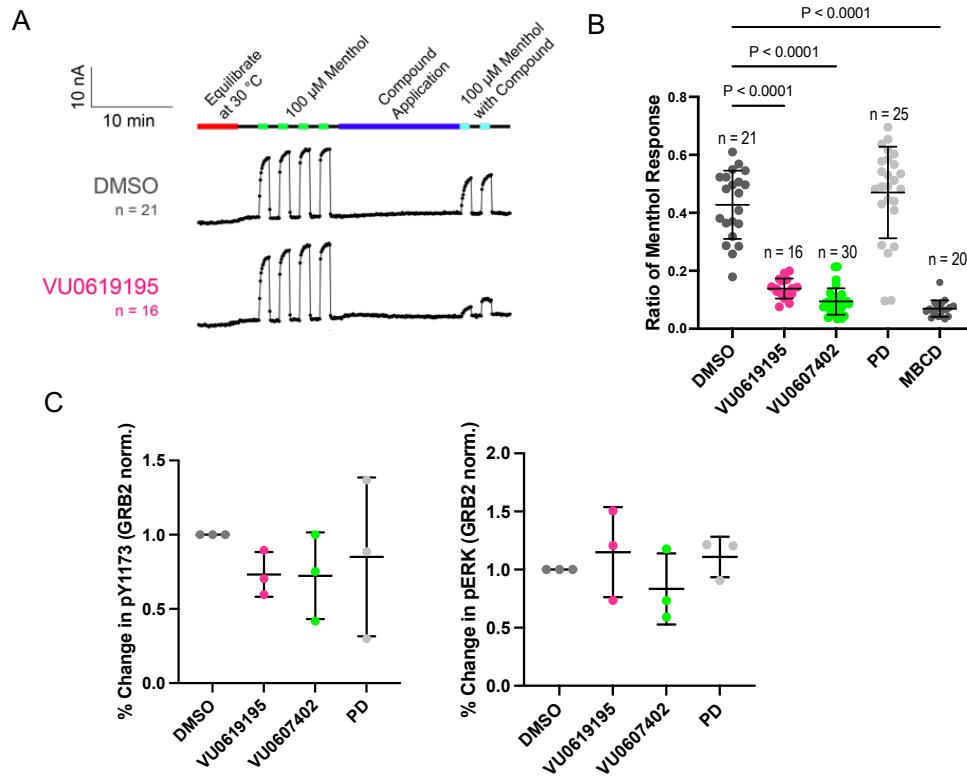


Figure 6. Class I and Class II compounds alter activity of TRPM8 but not EGFR. A) The average current traces of TRPM8 menthol response before and after exposure to the compounds in stably expressing full-length human TRPM8 HEK293T cells. Each dot is when the pulse program is applied. No perfusion was done in the first 5 minutes of the experiment to equilibrate the automated patch clamp plate to 30 °C. Menthol was applied at 100 μ M for 75 seconds 4 times to allow the menthol response to saturate before perfusing continuously either 0.03% DMSO (control), 10 μ M VU0619195 for 15 min (See Supp. Fig. 8A for VU0607402, PD and MBCD). 0.03% DMSO concentration was kept consistent throughout the experiment. Menthol was then applied at 100 μ M with the corresponding compounds twice for 75 seconds. Each n refers to the single sum of 20 cells from an amplifier on the automated patch clamp ensemble plate. **B)** The average ratio of menthol response from each compound in stably expressing full-length human TRPM8 HEK293T cells. The ratio of menthol response uses the data from panel A and (fig. S8A), where the last two menthol response before compound application were averaged and compared to the two menthol response after compound application. Each n refers to the single sum of 20 cells from an amplifier on the automated patch clamp ensemble plate and are jittered. P-values were determined by ANOVA followed by Dunnett's tests. Bars are means \pm SD. **C)** Results of Western blot analysis of phospho-EGFR (left) and ERK (right) from HeLa cells treated with compounds for 15 min then stimulated with EGF for 1 min. n =3, bars are means \pm SD. All comparisons are not significant.

Table 1. Protein-dependent compound structures and parameters

935

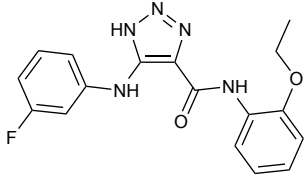
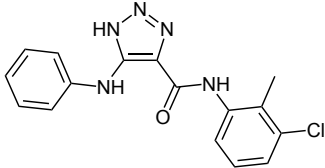
| VU# | Structure | cLogP | FSP3 | TPSA |
|-----------|---|-------|------|-------|
| VU0615562 |  | 3.93 | 0.12 | 91.93 |
| VU0619195 |  | 4.49 | 0.06 | 82.7 |

Table 2. Protein-independent compound structures and parameters

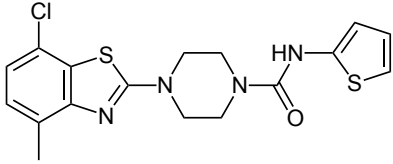
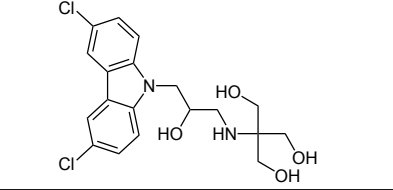
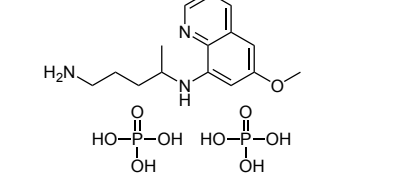
| VU# | Structure | cLogP | FSP3 | TPSA ⁰³⁶ 937 938 |
|------------------------|---|-------|------|-----------------------------------|
| VU0519975 |  | 4.4 | 0.29 | 104.95 |
| VU0607402 |  | 4.39 | 0.37 | 97.88 |
| Primaquine Diphosphate |  | 2.2 | 0.38 | 60.2 |

Table 3. Summary of biophysical effects of Class I and II compounds

| Compound | Class | Impact on $P_{\text{ordered, PMP22}}$ | Impact on $P_{\text{ordered, MAL}}$ | Impact on raft formation | Impact on raft formation modified by proteins? |
|------------------------|-------|--|-------------------------------------|--------------------------|--|
| VU0615562 | I | ↓ | ↓ | ↓ | Yes |
| VU0619195 | I | ↓ | ↓ | ↓ | Yes |
| VU0519975 | II | ↓ (borderline statistical significance) ^a | no change | ↓ | No |
| VU0607402 | II | ↓ (borderline statistical significance) ^a | no change | ↓ | No |
| Primaquine Diphosphate | II | ↑ ^b | ↑ | ↑ | No |

- a. A statistically significant decrease is clear in GPMVs RBL cells (fig. S1A), but is borderline in HeLa cells (Fig. 4A).
- b. A statistically significant increase is seen in GPMVs from HeLa cells (Fig. 4A) but not RBL cells (fig. S1A).